IUST
Iran University of
Science and Technology

Iranian Journal of Electrical and Electronic Engineering

Journal Homepage: ijeee.iust.ac.ir

The Dynamics of (5G) Millimeter Wave Energy Absorption in Human Tissue: A Comprehensive Analysis at the Free Space - Human Skin Interface

Godday Biowei*, Sulaiman A. Adekola**(C.A.) and Kamoli A. Amusa***

Abstract: This paper investigates the dynamics of mmWave at the free space-human skin interface. The four Fresnel equations tailored for parallel and perpendicular polarizations, are employed in the analysis. The research reveals that for human tissue with relative permittivities (18.99, 15.51, 13.35, 11.69, 10.40) and conductivities (22.48, 27.09, 29.76, 31.79, 33.38) S/m, when exposed to 5G mmWave frequencies (24, 30, 35, 40, 45) GHz, respectively, exhibits Brewster angles of $(79°, 78°, 77°, 76°, 75°)$, respectively. Additionally, it is shown that Brewster angles exist between $60°$ and $80°$, which aligns with existing literature using Gabriel's skin model. To further validate obtained results, use is made of the results of the Gabriel's skin model at (40, 60, 80, 100) GHz with the respective permittivities and conductivities, to generate new power reflection coefficients for the parallel and perpendicular polarizations for the sake of comparative analysis. First, comparisons of the curves for the Gabriel's skin model reported in the literature with this work, show fairly good agreements. Second, the Brewster angles of $(78°, 76°, 74°, 73°)$ obtained from this work, for the respective frequencies compare favorably with $(75°, 74°, 70°, 69°)$ extracted from Gabriel's skin model curves reported in the literature, with all values falling within the expected range of $60°$ to $80°$.

Keywords: 5G mmWave, Fresnel equations, human tissue, Brewster angle

1 Introduction

THE investigation carried out here is motivated by growing concerns about the impact of how the mmWave (5G) penetrates the human tissue through the skin causing some deleterious effects. It is recognized that wireless telecommunication devices have revolutionized global connectivity, yet they stand as the primary source of electromagnetic (EM) radiations today. The human body's absorption of these radiations poses potential risks, thus leading to neural effects and the development of cancer [1]. Other uncontrolled exposures can affect the central nerve system [2], [3]. Despite the hazards and the harmful trappings of the EM radiations, there are numerous benefits of the radiations [4]. Most widely utilized EM radiations worldwide are within the 100 kHz – 300 GHz band. Applications beneficial to mankind include mobile phones, medical/ industrial applications, medical diagnostics and therapy.

What has received considerable attention in the literature is the RF energy below 10 GHz in contrast with the scanty focus on 5G mmWave frequencies. There has been insufficient analytical study in the literature on 5G mmWave impact on the human skin, particularly at frequencies above 10 GHz. Therefore, we focus attention on frequencies above 10 GHz by

Iranian Journal of Electrical & Electronic Engineering, 2024.
Paper first received 11 April 2024 and accepted 15 June 2024.
* The author is with the Department of Electrical and Electronic Engineering, Niger Delta University, Wilberforce Island, Nigeria.
E-mail: biogod@ndu.edu.ng.
** The author is with the Department of Electrical and Electronic Engineering, Federal University, Otuoke, Nigeria.
E-mails: adekolaadeniyi43@gmail.com.
*** The author is with the Department of Electrical and Electronics Engineering, Federal University of Agriculture, Abeokuta, Nigeria
E-mail: amusaka@funaab.edu.ng.
Corresponding Author: Sulaiman A. Adekola.

selecting 5G mmWave frequencies given as (24, 30, 35, 40, 45) GHz. Major interest here is to investigate what happens when 5G mmWave strikes air-skin interface. That is to say, the activities begin at the surface.

It is worth pointing out here, *ab initio*, why we focus attention on the interface. The significance of the skin lies in its crucial role as a component that not only contains and protects the body but also establishes an impermeably flexible barrier between the external environment and the intricately regulated internal systems. It contributes to temperature regulation, immune defense, and the production of sensory experiences. The skin consists of epithelial tissue, covering the body's surface and lining various internal passages. Muscle tissue includes both striated (voluntary) muscles responsible for skeletal movement and smooth muscles, such as those surrounding the stomach.

Owing to the electrical characteristics of the human tissue, 5G mmWave interacts with it in three ways: transmission, reflection and absorption. It proves adequate then to split the investigation into two interrelated and significant aspects. Consequently, the investigation leverages the activities at the air-skin interface to two angles identified as *Brewster and critical* angles which exhibit some singular interesting characteristics. First, we start with the Brewster angle and we treat the critical angle thereafter.

Brewster angle can be used to investigate the behavior of plane thermal waves as they encounter the interface between different media. This application has been explored elsewhere [5]. The Brewster angle, characterized by zero reflection, is found to be applicable only under specific combinations of the diffusivity and thermal conductivity for both the incident and transmission media. What had been explicitly studied hitherto, are the experimental and theoretical investigations of thermal wave propagation produced by time-dependent heat sources [6], [7]. It has been investigated how thermal resistance can affect energy transmission across a boundary thereby setting a threshold over which the effect can be ignored [8]. Cancellation of reflection is the sole determinant on which the existence of Brewster's angle depends.

Although the concept of Brewster angle is conventionally associated with electromagnetic wave propagation, it is also applicable to other types of time-harmonic waves such as mechanical waves in elastic media [9], [10]. While the Brewster angle can be employed when considering thermal waves, evidence of such applicability is scanty, although thermal Brewster angle has been used in non-destructive testing [11]. Indeed, non-destructive evaluation has been achieved through what is known as thermal diffusivity relating to thermographic imaging [12], as well as thermal sensing [13] including thermal invisibility [14]. In dealing with physical systems, what is vital is a better understanding of the heat transfer between adjacent media in the direction normal to the interface and across all angles of incidence. A fundamental idea to be borne in mind is the notion of angle-dependent characteristics of thermal waves when considering the issue of complex structures in which the situation of two-dimensional models arises so as to understand how heat flow propagates across the media [15]-[17].

When use is made of the Brewster effect, it has been shown how optical image edge detection for amplitude and phase objects can be performed. Experimental validation has established how the orientation of amplitude and phase gradients within objects influence the directionality of the image transformation [18]. In the realm of analog image processing, investigators have paid attention to this in the literature. What has been described in [19] is the implementation of optical differentiation based on the excitation of what is known as surface plasmon polariton modes in Kretschman configuration [19]. Hitherto, image edge detection has been carried out using resonant structures for the situation of monochromatic light [20]. An experimental validation carried out in [21] borders on the application of the Brewster angle to optically detect edges in images of both phase and amplitude objects, although the application is limited to beams propagating in the plane of incidence [21].

Critical angle is of great practical utility which has been explained in several scientific studies exemplified by the usage in clinical sciences among others. The basic application borders on the knowledge of refractive index measurements concerning electrical parameters of the human tissue. Those electrical parameters are identified as the relative permittivity and conductivity of the human tissue. Practical measurements are classified by what is known as "*in vivo*" measurements. Samples of work done in the literature about the aforementioned parameters of the human tissue are exemplified in what follows. More specifically, human tissue samples have been used in refractive index measurements [22]. Also considered, are the optics of the human skin, human skin *in vivo* determination of the micro-spectroscopy of the skin, refractive indices estimation at eight wavelengths, complex refractive index measurements of biological tissues, experimental refractive index measurements of biological tissues as well as modified refractive index measurements and the use of confocal microscopy to measure refractive index of tissues [23]-[30]. Other authors addressed the use of optical coherence tomography, in consideration of wave penetration, therapeutic applications and penetration through stratum

cornea [31]-[34].

A detailed application of critical angle when used in refractive index measurement "*in vivo*" under partial contact of the skin, has been extensively investigated [35]. In [35], the authors precisely determined through experimental measurements, that the refractive index (RI) values are within 1.51 to 1.53 ($n = 1.51$ to $n = 1.53$) at the wavelength of 550 nm. Since refractive index is given by $n = \sqrt{\varepsilon_r}$, which means within relative permittivity of 2.28 to 2.34 ($\varepsilon_r = 2.28$ to 2.34). It ought to be noted that 550 nm ($f = 5.45 \times 10^{14}$ Hz) is the wavelength of yellow light. It is equally worth remarking that RI describes the status of the skin. Consequently, knowledge of n is essential for the evaluation of the characteristics of the human skin. Since the epidermis is the closest layer to the skin surface, it is logical to use the epidermis to measure the RI of the human tissue. In this wise, an average proves admissible for this purpose. Thus, use can be made of the upper and lower surfaces of the epidermis. In that way, what are applied, are the physical and optical distances between the interfaces. This is just one method. The second method involves the interrelationship between critical angle and the reflectance. Reflectance is the ratio of the intensity of reflected radiation to that of the radiation incident on a surface. This method is more effective than the first method because it makes use of the ratio of the surface and interior reflections [35].

Finally, it is worth pointing out here that microwave frequencies relate to electromagnetic waves with frequencies ranging from 300 MHz to 300 GHz. This frequency range has numerous applications, including radar systems, wireless communications, and medical imaging. In [36], the authors investigated the effects of microwave frequencies in the range 41.650 GHz to 41.795 GHz on human cells. The study revealed that, there are no significant effects on the cells when exposed to those frequencies. It is shown in [37] that at the air-skin interface about 26-41% of the normal incident wave is reflected. In [38], it was also stated that between 30-40% of microwave at 60 GHz is reflected at the air-skin interface; while [39] showed that 90% of microwave energy impinging the human body is absorbed by the skin. At the two frequency domains, the changes concern the electrical parameters which are the permittivity and conductivity. At the lower frequencies, the permittivity of the tissue is greater than the conductivity, while at the higher frequencies the conductivity is greater than permittivity

The analysis articulated in this paper begins by outlining the development of the plane wave around the skin using Maxwell's equations. Upon hitting the skin surface, part of the wave is reflected while the rest is transmitted. Fresnel's equations at the air-skin interface are used to derive expressions for the power reflection coefficients for both parallel and perpendicular polarizations. These coefficients for parallel polarizations help determine the Brewster angles of interest. Electrical parameters (ε_r, σ) for the frequencies 24, 30, 35, 40, and 45 GHz are sourced from the ITIS Foundation website [40] which is more comprehensive than those provided by FCC (Federal Communications Commission) [41]. The skin model applied is homogeneous and assumes no multiple reflections, allowing for the calculation of the Brewster angles. The study is then compared with the seminal work of Wu et al. [42] to validate the findings. However, Wu et al. used Gabriel's skin model and a different frequency range of 40, 60, 80, and 100 GHz. Since Wu et al. did not provide the necessary electrical parameters, we used the ITIS Foundation website [40] again to obtain the corresponding parameter for their frequency range. This method enabled reasonable comparisons between our results and the power reflection coefficients profiles reported by Wu et al.'s [42] for parallel polarization. The Brewster angles were extracted from Wu et al.'s [42] data. Additionally, we computed the perpendicular polarization power reflection coefficients in our study and compared the results with those of Wu et al.'s [42]. All comparative analyses showed fairly good agreements.

The paper is organized as follows: Section 1 provides an introduction. Section 2 explores the dynamics of 5G mmWave at the air-human skin interface, beginning with the decoupling of Maxwell's equations and describing the adopted model, followed by an introduction to Fresnel's equations relevant to interface events such as normalized power reflection coefficients, Brewster angles, and critical angles. This section also outlines the significance of the Specific Absorption Rate (SAR). Section 3 presents a thorough discussion of results, including validation. Section 4 offers concluding remarks, highlighting the main contributions.

2 Unraveling the dynamics of (5G) mmWave at the air-human skin interface Fonts

Investigating the behavior of (5G) mmWave frequencies at the interface between air and human skin involves understanding the EM environment surrounding the skin. This environment adheres to Maxwell's equations, describing a source free and charge-free medium.

2.1 Decoupling Maxwell's equations and solution for (E, H) fields

When source-free and charge-free Maxwell's equations are decoupled, they yield second-order partial differential equations for the electric ($\overline{\mathrm{E}}$) and magnetic

($\overline{H}$) fields, respectively, representing the propagation of these fields in free space with constant velocity with no acceleration. Thus, decoupling Maxwell's equations gives rise to a second-order partial differential equation for the electric field vector, given as

$$\nabla^2\overline{E} - \mu_0\varepsilon_0\frac{\partial^2\overline{E}}{\partial t^2} = 0 \tag{1a}$$

and

$$\nabla^2\overline{H} - \mu_0\varepsilon_0\frac{\partial^2\overline{H}}{\partial t^2} = 0 \tag{1b}$$

for the magnetic field vector, where the phase velocity assumes a form expressed as $v_p = 1/\sqrt{\mu_0\varepsilon_0}$, in which (μ_0, ε_0) are the permeability and dielectric permittivity of free space, respectively.

Each of eqs. (1a) and (1b) is homogeneous vector Helmholtz equation that is equivalent to three scalar wave equations, one for each component along $x-$, $y-$ and $z-$ directions. Without loss of generality, suppose the wave propagates along the positive $z-$ direction such that $\overline{E}$ has only $x-$ component, then

$$\overline{E} = \hat{x}E_x(z) \tag{2}$$

Use of eqs. (2) and (1a) yields:

$$\frac{\partial^2 E_x(z)}{\partial z^2} - \beta^2 E_x(z) = 0 \tag{2a}$$

Equation (2a) is a scalar wave equation, a linear homogeneous partial differential equation whose solution is

$$E_x(z) = E_0 e^{-j\beta z} + E_0' e^{j\beta z} \tag{2b}$$

where E_0 and E_0' are constants

Since the wave is assumed propagating in the positive $z-$ direction, $E_0' = 0$, so that eq. (2b) reduces to

$$E_x(z) = E_0 e^{-j\beta z} \tag{2c}$$

Inserting exp (jωt) time variation that is earlier suppressed,

$$\begin{aligned}\overline{E}(z,t) &= \sqrt{2}\mathrm{Re}[E_x(z)e^{j\omega t}\hat{x}] \\ &= \sqrt{2}\mathrm{Re}\left[E_0 e^{j(\omega t-\beta z)}\hat{x}\right]\end{aligned} \tag{3}$$

or

$$\overline{E}(z,t) = \sqrt{2}E_0\cos(\omega t - \beta z)\hat{x} \tag{4}$$

and

$$\overline{H}(z,t) = \sqrt{2}H_0\cos(\omega t - \beta z)\hat{y} \tag{5}$$

provided $(\hat{x}, \hat{y})$ are unit vectors in the $x-$, $y-$ directions, respectively, and where the amplitudes are related by

$$H_0 = \frac{E_0}{\eta_0} \tag{6}$$

and

$$\eta_0 = \sqrt{\frac{\mu_0}{\varepsilon_0}} \tag{6a}$$

provided η_0 is the intrinsic impedance of free space.

Thus, $(\overline{E},\overline{H})$ fields whose solutions are given by eqs. (4) and (5), respectively, are the oscillating waves in free space, which is the environment where the human skin lies. These are waves impinging on the surface of the skin.

It is now necessary to briefly discuss the model adopted for the problem, which is considered in what follows.

2.2 The Model

The model depicted in Figure 1 demonstrates the propagation of EM waves at an oblique angle of incidence. It includes layers of human skin to align with the primary focus of the paper's analysis. For simplicity, a hypothetical interface is considered, ignoring certain effects like thermal resistance. The model also assumes uniform electrical properties (permittivity and conductivity) throughout the skin, eliminating the need to account for possible multiple reflections at the skin layer boundaries. Essentially, the body tissue is assumed to be homogeneous, excluding the lower layers of the skin, the thickness of the layers, and the effects of sub-reflections from the interface of the lower epidermis layers. The next phase involves analyzing the dynamics of electromagnetic wave energy at the air-skin interface, which includes examining the Fresnel equations.

2.3 Fresnel Equations

Investigated here, to examine what happens when the oscillating wave expressed by eq. (4) strikes the human skin at air-skin junction, is the dynamics of mmWave at the interface. This presents a boundary-value problem requiring a solution through appropriate boundary conditions. Fig. 1 depicts the necessary oblique incidence wave scenarios where Fig. 1(a) represents perpendicular polarization while Fig. 1(b) describes the situation for parallel polarization. The electric field is taken as the reference field. Consequently, polarization is defined with respect to the electric field. Thus, perpendicular polarization is where electric is perpendicular to the plane of incidence. With this background established, one is now in a suitable position to fully consider the analysis of oblique incidence, which is of practical interest in this paper.

As in Euclidian geometry $(\overline{E}_\perp, \overline{H}_\perp)$ stands for perpendicular polarized fields identified by the subscript $(\perp)$, while $(\overline{E}_\parallel, \overline{H}_\parallel)$ represents parallel polarized fields typified by the subscript $(\parallel)$. Two boundary conditions are imposed on the air-skin interface. These are: tangential $\overline{H}$ is continuous across the boundary and tangential $\overline{E}$ is also continuous across the boundary. A straightforward algebraic manipulation leads to the emergence of the famous Fresnel equations expressible in forms given as [42]:

$$\Gamma_\perp = \frac{\overline{E}_\perp^r}{\overline{E}_\perp^i} = \frac{\cos\theta_i - \sqrt{\varepsilon_r - \sin^2\theta_i}}{\cos\theta_i + \sqrt{\varepsilon_r - \sin^2\theta_i}} \tag{7}$$

$$\tau_\perp = \frac{\overline{E}_\perp^t}{\overline{E}_\perp^i} = \frac{2\cos\theta_i}{\cos\theta_i + \sqrt{\varepsilon_r - \sin^2\theta_i}} \tag{8}$$

$$\Gamma_\parallel = \frac{\overline{E}_\parallel^r}{\overline{E}_\parallel^i} = \frac{-\varepsilon_r\cos\theta_i + \sqrt{\varepsilon_r - \sin^2\theta_i}}{\varepsilon_r\cos\theta_i + \sqrt{\varepsilon_r - \sin^2\theta_i}} \tag{9}$$

$$\tau_{\parallel} = \frac{\overline{E}_{\parallel}^{t}}{\overline{E}_{\parallel}^{i}} = \frac{2\cos\theta_i}{\varepsilon_r \cos\theta_i + \sqrt{\varepsilon_r - \sin^2\theta_i}} \quad (10)$$

provided $(\Gamma_{\perp}, \tau_{\perp})$ stand for the reflection and transmission coefficients for the perpendicular polarization, respectively, while $(\Gamma_{\parallel}, \tau_{\parallel})$ are the reflection and transmission coefficients for parallel polarization, respectively; $\overline{E}^{i}$, $\overline{E}^{r}$ and $\overline{E}^{t}$ stand for the incident, reflected and transmitted electric fields, respectively, ε_r is the relative permittivity of the human skin and θ_i is the angle of incidence of the wave at the interface. When use is made of eqs. (7) – (10), the reflected components of the incident wave at the interface leads to an expression given as

$$\overline{E}^{r} = \Gamma \overline{E}^{i} \quad (11)$$

while the transmitted component provides an expression cast as

$$\overline{E}^{t} = \tau \overline{E}^{i} \quad (12)$$

where Γ assumes expressions in eqs. (7) and (9) for perpendicular and parallel polarized incident waves, respectively, and τ assumes the forms given by eqs. (8) and (10) for the perpendicular and parallel polarized incident waves, respectively.

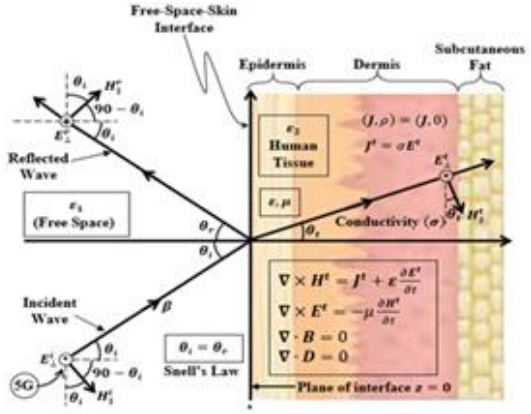

(a)

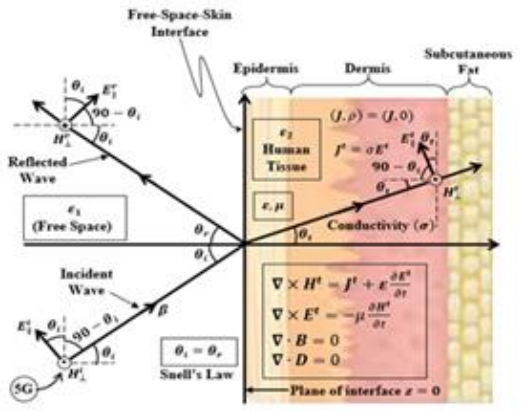

(b)

Fig. 1 Oblique incident 5G mmWave polarization at the interface (a) perpendicular (b) parallel

2.4 Normalized Power

The instantaneous power radiated by an EM wave is generally expressed as,

$$\overline{P} = \overline{E} \times \overline{H}^{*} = \frac{\overline{E}^{2}}{\eta} \quad (13)$$

where $(*)$ represents the conjugate notation. In eq. (13), $(\overline{E}, \overline{H})$ stand for the instantaneous electric and magnetic field vectors, respectively, and η represents the intrinsic impedance of the medium. Thus, the normalized power related to both the reflected and transmitted waves at the interface can be quantitatively articulated in the following form:

$$P_n = (\Gamma)^2 \quad (14)$$

for the normalized reflected power and for normalized transmitted or absorption power,

$$P_n = (\tau)^2 \quad (15)$$

provided P_n represents normalized power in eqs. (14) and (15), Γ stands for eq. (7) or (9) (i. e. $\Gamma_{\perp}$ or $\Gamma_{\parallel}$); and τ represents eq. (8) or (10) (i. e. $\tau_{\perp}$ or $\tau_{\parallel}$).

In this paper, the interest is in the reflected power and not the transmitted or absorbed power which shall be the focus of the companion Paper II to follow in the near future. Perhaps it will not be amiss to state that, the portion of the incident wave absorbed is embedded in the human tissue. It should be understood that to estimate the amount of EM energy absorbed requires the knowledge of the electrical parameters of the human tissue.

The situation that is of interest here is what is addressed in what follows.

2.5 Brewster and Critical Angles at the Interface

Brewster angle denoted by θ_B, is associated with parallel polarization which is fully represented in the oblique incidence depicted in Fig. 2(a).

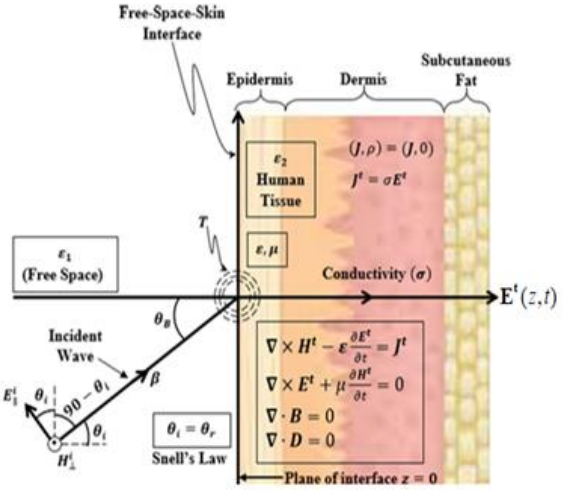

(a)

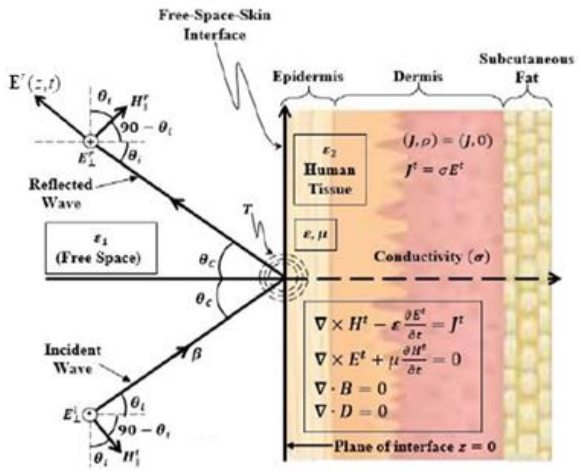

(b)

Fig. 2 Events at the boundary of air-skin interface (a) Brewster angle at the interface for parallel polarization (b) Critical angle at the interface for perpendicular polarization

In that figure, the total EM wave is transmitted without reflections at the Brewster angle. What happens before reaching the Brewster angle and thereafter, is worthy of investigation. For this purpose, the relevant forms of the equations derived in section 2.3 are needed here for the purpose of analytical investigations. Thus, use is made of eqs. (9) and (14) to generate the design curves for the normalized reflected power.

2.6 "*In vivo*" Electrical Parameter Measurements

"*In vivo*" measurements of the electrical parameters of the human tissue can be affected through the use of radio frequency (RF) reflected power and the critical angle concept. Experimental refractive index and conductivity measurements of the human skin have been achieved through the use of reflectometers and vector network analyzers or reflected RF energy from the skin [35]. Examples abound in the literature. Using partial contact of the skin [35] provides how a refractive index within 1.51 to 1.53 has been achieved. This corresponds to relative permittivity within 2.28 to 2.34.

As stated earlier, there is a temperature gradient, symbolized by T in Fig. 2, at the point of contact on the human skin where RF energy strikes the skin. Analysis of heat conduction process is essential in such a situation. In [5], it has been stated that the heating process at the interface when such condition occurs, follows a diffusion equation given as:

$$\nabla^2 \mathrm{T}(\mathrm{x}) = \frac{1}{\mathrm{D}} \frac{\partial}{\partial \mathrm{t}} \{\mathrm{T}(\mathrm{x}, \mathrm{t})\} \tag{16}$$

provided $\mathrm{T}(\mathrm{x}, \mathrm{t})$ is the time-dependent temperature distribution function while D stands for diffusivity of the medium. One can readily see that eq. (16) is a Laplacian equation which can be solved by well-known methods. In the usual case of time-harmonic wave as applicable here with $\exp(\mathrm{j}\omega \mathrm{t})$ time variation such that

$$\mathrm{T}(\mathrm{x}, \mathrm{t}) = \mathrm{Re}[\mathrm{T}(\mathrm{x}) \mathrm{e}^{\mathrm{j}\omega \mathrm{t}}] \tag{17}$$

then eq. (16) is expressible in the frequency domain in a form given as

$$\nabla^2 \mathrm{T}(\mathrm{x}) = \omega^2 \mathrm{T}(\mathrm{x}) \tag{18}$$

where, ω is the angular frequency in radians and the $\exp(\mathrm{j}\omega \mathrm{t})$ time variation has been suppressed. Details of the solution can be found elsewhere [5].

2.7 Specific Absorption Rate (SAR)

The Specific Absorption Rate (SAR) measures the rate at which RF energy is absorbed per unit mass by a human body when exposed to a Radio Frequency (RF) EM field. It is quantitatively expressed in a form given as Wu et al, [42]-[43].

$$\mathrm{SAR} = \frac{\mathrm{P_{diss}}}{\mathrm{m}} = \frac{\sigma |\mathrm{E}|^2}{\rho} \tag{19}$$

provided $\mathrm{P_{diss}}$ (W) is the power dissipated in the tissue, m is the tissue mass (kg) under exposure, σ is the conductivity [in Siemens/meter (S/m)] of the tissue, ρ is the tissue mass density (kg/m^3) and E is the root mean square value of the electric field strength (V/m) dissipated in the tissue.

SAR is measured in watts per kilogram (W/kg). Its value cannot exceed 2 W/kg, with a limit of 1.6 W/kg for mobile devices. It is important to note that in this eq. (19), E, σ and ρ are functions of the position within the tissue, which is beyond the scope of this paper but will be addressed in a forthcoming companion paper.

This paper primarily focuses on the refection coefficient at the skin surface for evaluating Brewster angle, which is its main objective. However, a brief discussion of SAR is provided here. SAR involves the dynamics within the tissue structure, primarily concerning the transmitted electric field. The transmitted electric intersects with the tissue's conductivity, inducing the conduction current density $\bar{\mathrm{J}} = \sigma \bar{\mathrm{E}}$ which makes Maxwell's equations inside the tissue inhomogeneous. These inhomogeneous Maxwell's equations are evident in the internal structure of the model shown in Figs. 1 and 2. Decoupling Maxwell's equations provides a solution to the electric field associated with the propagation parameters α (attenuation constant) and β (propagation wave number). Consequently, penetration depth δ is expressible in a form given as;

$$\delta = \frac{1}{\alpha} \tag{20}$$

Equation (20) along with the usual expression for the power density (PD) radiated by a transmitting antenna at the far-field distance d, can be used to evaluate SAR. The power density (PD) is given as [42].

$$\mathrm{PD} = \frac{\mathrm{G_t P_t}}{4\pi \mathrm{d}^2} \tag{21}$$

where G_t is the transmitting antenna gain, P_t (W) is the total power fed into the antenna and d(m) is the distance from the radiation source.

MATLAB simulations of the electric field can demonstrate how the damped oscillating transmitted wave behaves within the internal structure of the skin, comprising the epidermis, dermis and hypodermis with the following dimensions [44]:

Epidermis: (0.006 – 0.1) mm
Dermis: (1.2 – 2.8) mm
Hypodermis (subcutaneous tissue): (1.1 – 5.6) mm

This gives a total of 8.5 mm for the three layers.

These topics will be thoroughly discussed in the upcoming companion paper, which falls outside the scope of this current work. That paper will investigate how the Specific Absorption Rate (SAR) at the surface of exposed tissue compares to the SAR deeper within the tissue.

3 Results and Discussion

The numerical results presented here are derived from the equations established in section 2. Our primary objective is to illustrate the behavior of normalized power reflection coefficients at the interface between free space and human skin at five selected frequencies within the mmWave band: 24, 30, 35, 40, and 45 GHz. These frequencies are staggered 5 GHz apart to facilitate comparative analysis. Due to the limited availability of measured electrical parameters at these frequencies in existing literature, we utilized data provided by ITIS Foundation website [37] website. Figs. 3-5 display the computed profiles using pairs of relative permittivity and conductivity for these frequencies, as detailed in Table 1. Before discussing Figs. 3-5, it is essential to examine the entries in Table 1, which lists the electrical properties of three tissues: skin, kidney, and heart. Column 1 identifies the mmWave frequencies (24 to 45 GHz), and column 2 and 3 describe the permittivities and conductivities, respectively. The tissue Skin, Kidney and Heart are clearly indicated.

For the skin, the computed power reflection coefficients against the angle of incidence are plotted for each frequency (24, 30, 35, 40, 45 GHz) in Figs. 3(a) to 3(e). Each figure indicates the corresponding permittivity and conductivity, as wells as the frequency and tissue type. The Brewster angles, representing the turning points on the angle of incidence axis, and the critical angles are also highlighted and the numerical values are provided in Table 2. Notably, the critical angle for each of all five frequencies is 90°. Figs. 4(a) to 4(e) illustrate the same analysis for the kidney tissue, using the electrical parameters from Table 1.

As with the skin, Brewster angles and critical angles are identified in the figures, and the numerical values of Brewster angles are provided in Table 3. For the heart tissue, Figs. 5(a) to 5(e) show the profiles for the five frequencies, using the parameters from Table 1 and the numerical values of the Brewster angles are tabulated in Table 4. The descriptions of the design curves for skin and kidney apply similarly to the heart.

Table 1 Electrical Properties of Tissues [40]

Frequency (GHz)	Relative Permittivity	Conductivity (S/m)
	Skin	
24	18.99	22.48
30	15.51	27.09
35	13.35	29.79
40	11.69	31.79
45	10.40	33.38
	Kidney	
24	24.83	28.96
30	20.87	34.24
35	18.38	37.82
40	16.41	40.79
45	14.85	43.32
	Heart	
24	25.98	30.22
30	21.79	35.81
35	19.16	39.59
40	17.09	42.74
45	15.43	45.39

Further analysis involves comparing relevant parameters from Table 1. Table 2 details the refractive indices, Brewster angles, and critical angles for skin, showing that Brewster angles generally decrease with increasing frequency, while critical angles remain at 90°. Similar trends are observed for kidney and heart tissues in Figs. 4 and 5 as well as Table 3 and 4.

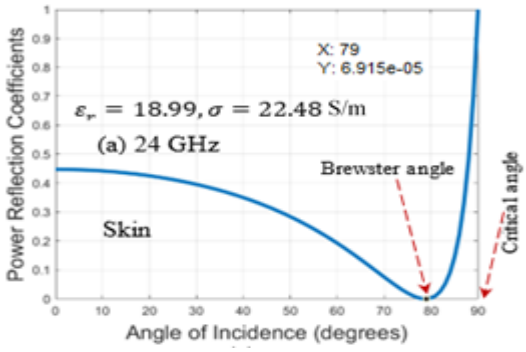

(a)

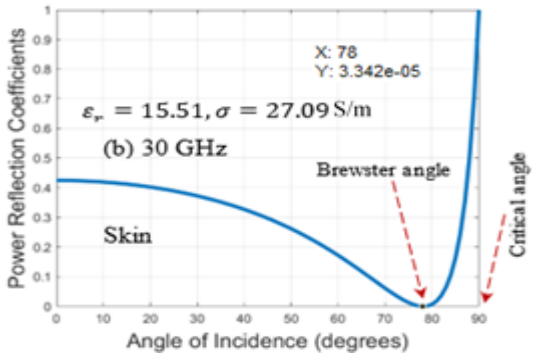

(b)

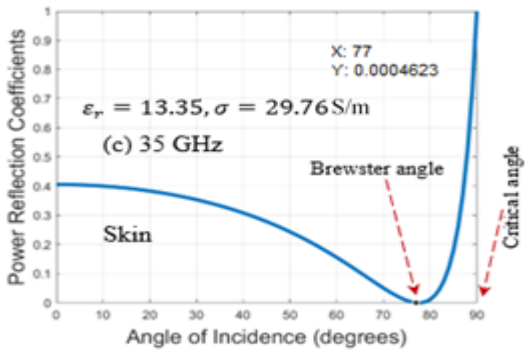

(c)

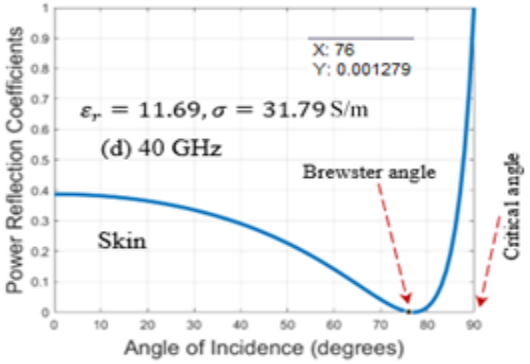

(d)

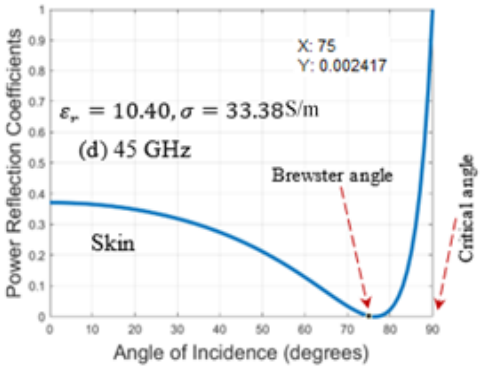

(e)

Fig. 3 Profiles of parallel polarized power reflection coefficients for the skin showing Brewster angles with permittivity ε_r: 18.99, 15.51, 13.35, 11.69 and 10.40. conductivity σ (S/m): 22.48, 27.09, 29.76, 31.79 and 33.38 at (a) 24 GHz (b) 30 GHz (c) 35 GHz (d) 40 GHz and (e) 45 GHz, respectively.

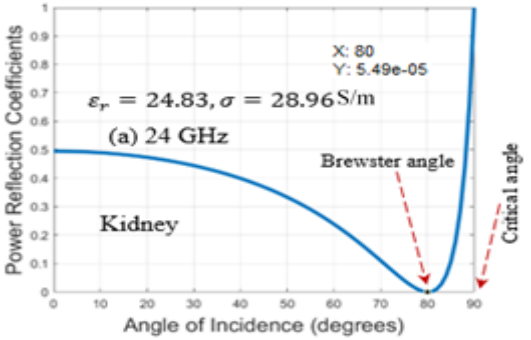

(a)

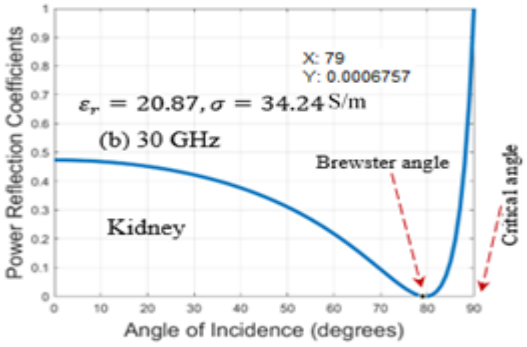

(b)

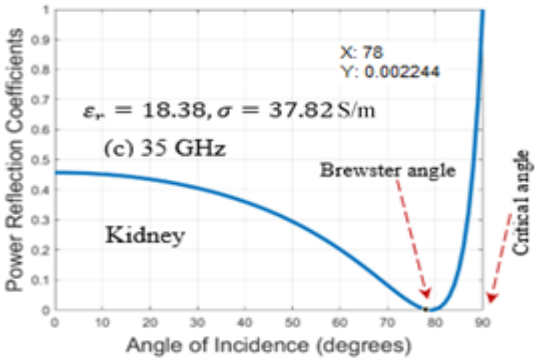

(c)

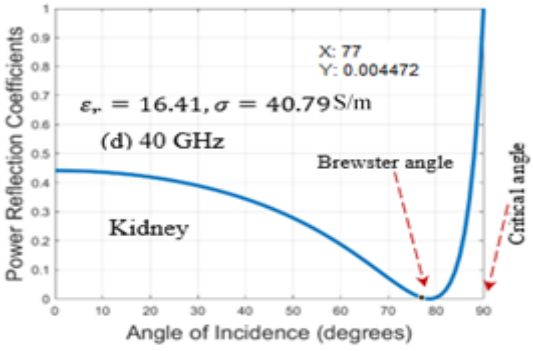

(d)

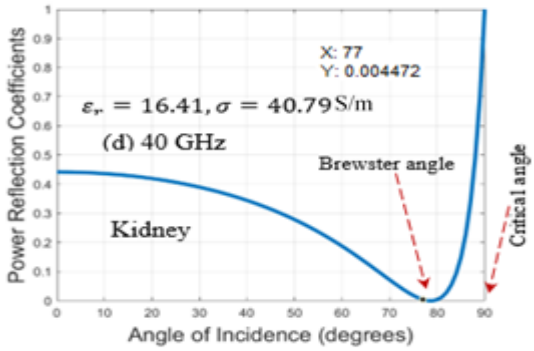

(e)

Fig. 4 Profiles of parallel polarized power reflection coefficients for the Kidney showing Brewster angles with permittivity ε_r: 24.83, 20.87, 18.38, 16.41 and 14.85. conductivity σ (S/m): 28.96, 34.24, 37.82, 40.79 and 43.32 at (a) 24 GHz (b) 30 GHz (c) 35 GHz (d) 40 GHz and (e) 45 GHz, respectively.

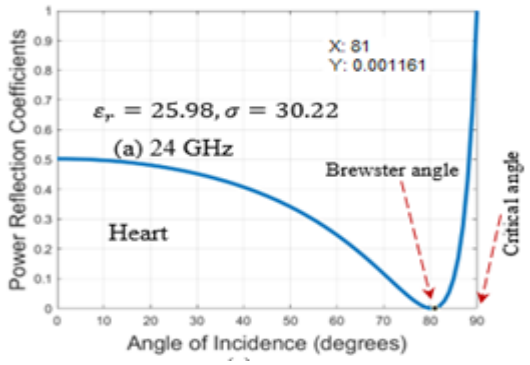

(a)

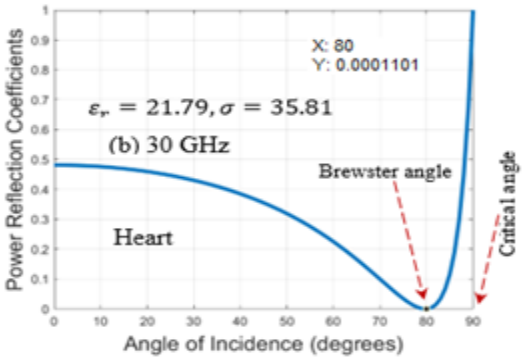

(b)

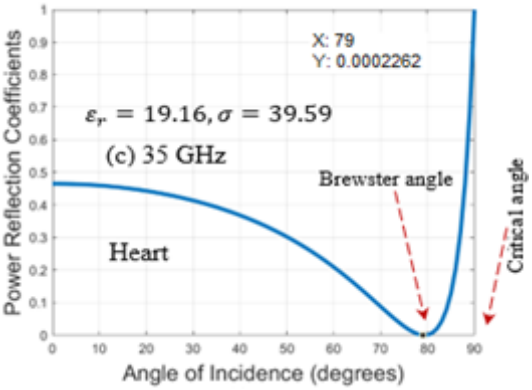

(c)

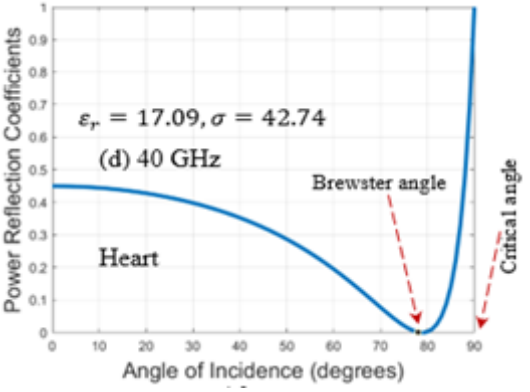

(d)

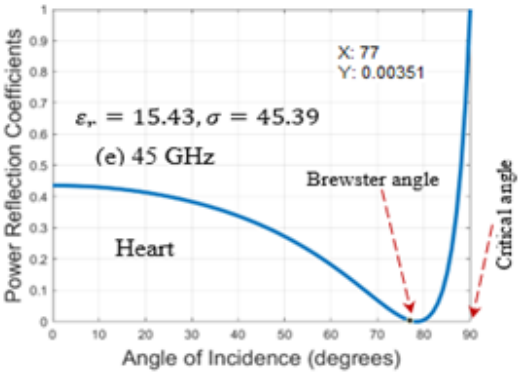

(e)

Fig. 5 Profiles of parallel polarized power reflection coefficients for the Heart showing Brewster angles with permittivity ε_r: 25.98, 21.79, 19.16, 17.09 and 15.43. conductivity σ (S/m): 30.22, 35.81, 39.59, 42.74 and 45.39 at (a) 24 GHz (b) 30 GHz (c) 35 GHz (d) 40 GHz and (e) 45 GHz.

As a further analysis, it is necessary to consider relative comparisons of relevant parameters that are germane to this paper. In this regard, use is made of entries of Tables 2, 3 and 4, which display comparative characteristics for the Skin, Kidney and Heart, respectively. Parameters spelt out in the tables are relative permittivity, conductivity, refractive index, Brewster critical angles for the five frequencies 24, 30, 35, 40 and 45 GHz used in this paper. It is clearly seen in those tabular presentations how values of the Brewster angles generally decreases with increasing operating frequencies, while the critical angles occur at 90° in all cases. Expectedly, the refractive indices also decrease with increasing frequencies.

We are now in a position to consider the validation of the results of this paper by comparisons with similar works in the literature. This is considered in what follows.

Presented in Table 2 are data extracted from Figs. 3(a) – 3(e) in relation to Brewster and critical angles of incidence for the skin. Also, Table 3 describe similar data entries for Kidney while Table 4 indicate those for the Heart.

Table 2 Brewster and critical angles associated with five different frequencies (Skin)

Frequency (GHz)	Skin				
	ε_r	$\sigma(S/m)$	n	θ_B	θ_c
24	18.99	22.48	4.36	79°	90°
30	15.51	27.09	3.94	78°	90°
35	13.35	29.76	3.65	77°	90°
40	11.69	31.79	3.42	76°	90°
45	10.40	33.38	3.23	75°	90°

Table 3 Brewster and critical angles associated with five different frequencies (Kidney)

Frequency (GHz)	Kidney				
	ε_r	$\sigma(S/m)$	n	θ_B	θ_C
24	24.83	28.96	4.99	80°	90°
30	20.87	34.24	4.57	79°	90°
35	18.38	37.82	4.29	78°	90°
40	16.41	40.79	4.05	77°	90°
45	14.85	43.32	3.85	76°	90°

Table 4 Brewster and critical angles associated with five different frequencies (Heart)

Frequency (GHz)	Heart				
	ε_r	$\sigma(S/m)$	n	θ_B	θ_C
24	25.98	30.22	5.09	81°	90°
30	21.79	35.81	4.67	80°	90°
35	19.16	39.59	4.38	79°	90°
40	17.09	42.74	4.13	78°	90°
45	15.43	45.39	3.93	77°	90°

3.1 Validation

The electrical parameters at the mmWave frequencies (24, 30, 35, 40, 45 GHz) for human tissue used in Table 1 were sourced from the ITIS Foundation website [40]. However, Wu et al. [42] used different frequencies (40, 60, 80, 100 GHz) for air-skin interface without providing their electrical parameters. They employed the Gabriel's skin model. Therefore, we obtain parameters for those frequencies as well, using ITIS Foundation data [40], as summarized in Table 5. For validation, we compared results for parallel and perpendicular polarizations.

3.1.1 Parallel Polarization

We compared results for parallel polarization using the frequencies from Wu et al. [42] and our derived parameters, shown in blue in Fig. 6, superimposed on Wu et al.'s characteristics. Table 3 compares percentage power reflections and Brewster angles from our computations with those extracted from Wu et al.'s curves. Our Brewster angles of $(78°, 76°, 74°, 73°)$ show a decrease with increasing frequency, aligning reasonably with their approximate values of $(75°, 74°, 70°, 69°)$. The critical angle remains at $90°$, while Wu et al.'s profiles [42] did not reach the critical angle. The agreement between our results and those of Wu et al. demonstrates the validity of our findings. Wu et al. [42] suggested Brewster angles should range between $60°$ and $80°$ for parallel polarization, and our results between $73°$ to $78°$ falls within this range.

3.1.2 Perpendicular polarization

For perpendicular polarization, we generated profiles using the electrical parameters from ITIS foundation [40] and compared the results with Wu et al.'s [42] results of (40, 60, 80, 100 GHz). Fig. 7 shows our computed profiles in blue, superimposed on Wu et al.'s [42] characteristics. The fairly good agreement between the profiles further validates our results.

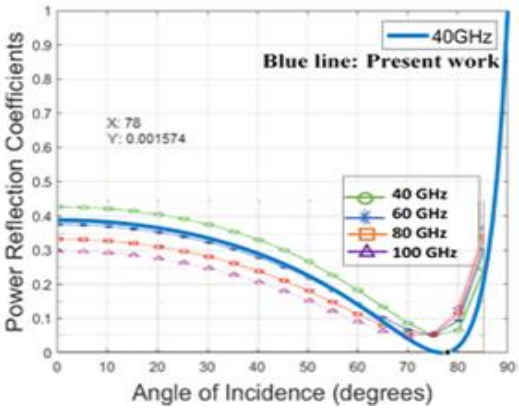

(a)

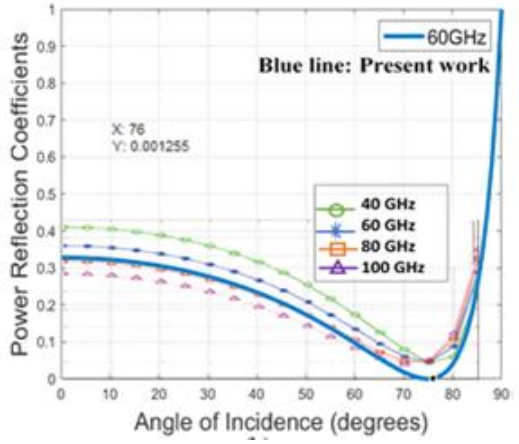

(b)

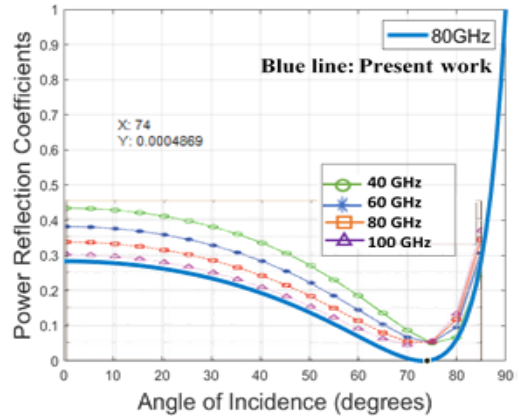

(c)

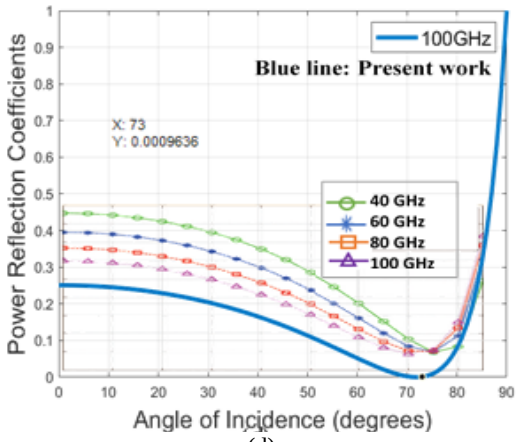

(d)

Fig. 6 Profiles of parallel polarization power reflection coefficients of this work compared with those in the literature [42, page 75, Fig. (5a) for Gabriel's skin model air-skin interface]

Table 5 Comparative Results of Power Reflection Coefficients and Brewster Angles

Frequency (GHz)	ε_r	σ (S/m)	% Reflection		Brewster Angle	
			This Work	[42]	This Work	[42]
40	11.69	31.79	39	43	78°	75°
60	7.98	36.39	32	38	76°	74°
80	6.39	38.39	29	34	74°	70°
100	5.59	39.43	26	30	73°	69°

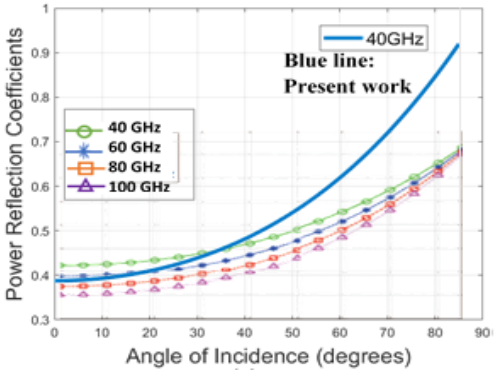

(a)

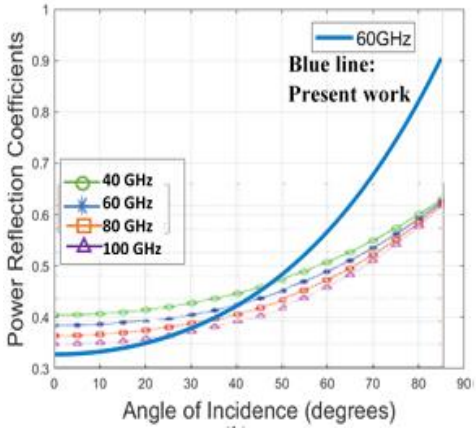

(b)

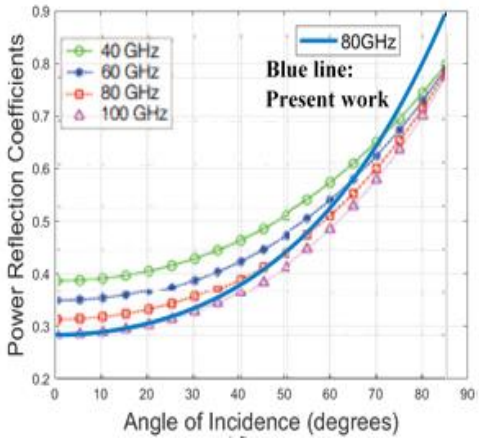

(c)

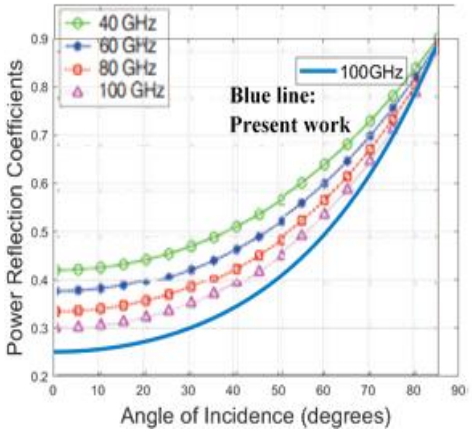

(d)

Fig. 7 Profiles of perpendicular polarization power reflection coefficients of this work compared with that in the literature [42, page 75, Fig. (5b) for Gabriel skin model air-skin interface]

4 Concluding Remarks

The free-space-human skin interface serves as a crucial boundary for predicting and understanding the behavior of mmWave within human tissue. This paper utilizes the four Fresnel equations for parallel and perpendicular polarizations to thoroughly examine this critical interface. The study reveals that human tissue with relative permittivities of skin (18.99, 15.51, 13.35, 11.69, 10.40) and conductivities (22.48, 27.09, 29.76, 31.79, and 33.38) S/m, when exposed to 5G mmWave frequencies (24, 30, 35, 40, 45) GHz, respectively, exhibits Brewster angles $(79°, 78°, 77°, 76°, 75°)$. Significantly, at these Brewster angles, all mmWaves penetrate the human tissue without reflecting off the skin surface – an innovative discovery highlighted in this paper. The Brewster angle is shown to decrease with increasing frequency. Other findings indicate similar characteristics across the 24 to 45 GHz mmWave frequency range. Additionally, Brewster angles between 60° and 80° are observed at various frequencies, where

the entire parallel polarization energy is absorbed by the human skin. This aligns with existing literature using Gabriel's skin model.

To further validate our results, we compared our findings with Gabriel's skin model at $(40°, 60°, 80°, 100°)$ GHz, using respective permittivities and conductivities to generate new power reflection coefficients for both polarizations. Comparisons of our curves with those from Gabriel's model show fairly good agreements. Our Brewster angles of $(78°, 76°, 74°, 73°)$ for the respective frequencies compare favorably with the $(75°, 74°, 70°, 69°)$ from Gabriel's model, all within the expected 60° to 80° range. A table of comparisons is provided for completeness. The differences can be attributed to the different models used.

Conflict of Interest

The authors declare no conflict of interest

Author Contributions

GB: original draft preparation, software & simulation;
SAA: idea & conceptualization, methodology, revise;
KAA: analysis, revise & editing

Funding

No funding was received for this work**.**

Informed Consent Statement

Not applicable

Acknowledgement

The insightful feedback from two anonymous reviewers significantly enhanced an earlier version of this paper. Their valuable comments are gratefully acknowledged.

References

[1] Batool S., Bibi A., and Mangini F., "Benefits and Hazards of Electromagnetic Waves, Telecommunications, Physical and Biomedical: A Review," *European Review for Medical and Pharmacological Science,* Vol. 23, pp. 3121-3128, 2019.

[2] Kim L.J., J.H. Kim, H.R. Kim and K. Kim, "Possible Effects of Radio Frequency Electromagnetic Field exposure on Central Nerve System," *Biomedical and Therapeutics* , Vol. 27, No. 3, pp. 265-275, 2019.

[3] Lin J.C., "Human Exposure to RF Microwave and millimeter Wave Electromagnetic Radiation [Health Effects]," *in IEEE Microwave Magazine,* Vol. 17, No. 6, pp. 32-36, 2016.

[4] Orlacchio R., Alekseev S.L., Drean Y Y., Sauleau R.L., Le Guerel. R., and Zhadobov M., "millimeter-Wave Pulsed Heating In Vitro: Cell Mortality and Heat Shock Response," *Scientific Reports.* Vol. 9, No. 15249, pp. 1-11, 2019.

[5] Romero-Ramos C.A., Manzanares-Martizez J.B., Soto-Puebla D., Morales-Morales G.A., and Rutz-Rosales C.E., "Brewster angle of thermal diffusivity waves at an interface," *Results in Physics,* Vol. 30, No. 104856, pp. 1-4, 2021.

[6] Nie B.D., and Cao B.Y., "Reflection of a thermal wave at an ideal interface," *Int. J. Heat Mass Trans,* Vol. 116, pp. 314-328, 2018.

[7] Sanchez-Perez C., De Leon-Hermandez A., and Garcia-Cadena C., "Optical device for thermal diffusivity determination in liquids by reflection of a thermal wave," *Rev. Sci Instrum,* Vol. 88, No. 8, p. 084901, 2017.

[8] Lor W., and Chu H., "Effect of interface thermal resistance on heat transfer in a composite medium using the thermal wave model," *Int. J. Heat Mass Transf,* Vol. 43, pp. 653-63, 2000.

[9] Born M., and Wolf, E., *Principles of optics electromagnetic theory of propagation, interference and diffraction of light*. Elsevier, 2013.

[10] Manzanares-Martinez, B., and Ramos-Mendieta, F., "Transverse eleastic waves in superlattices: The brewster acoustic angle,," *Physical Review,* Vol. 13, No. 19, p. 12877, 2000.

[11] Karam M.A., Volt C.H., and Meyer A.D., *Systems and methods for measuring at least one thermal property of materials based on a thermal brewster angle*. US Patent, 8(065):108, 2011.

[12] Farhat M., Chen P.Y., Bagel H., Amra C., Guenneau S., and Alu A., "Thermal invisibility based on scattering cancellation and mantle cloaking," *Sci Rep.,* Vol. 5, No. 1, pp. 1-9, 2015.

[13] Gavrilov D., Macy R.G., and Almond D., "A review of imaging methods in analysis of works of art: Thermographic imagnig method in art analysis," *Can. J. Phys.,* Vol. 92, No. 4, pp. 341-64, 2014.

[14] Reyes-Romero D., Behrmann O., Dame G., and Urban G., "Dynamic thermal sensor for biofilm monitoring," *Sens Actuators A,* Vol. 213, pp. 43-51, 2014.

[15] Qiu L., Scheider K., Radwan S.A., Larkin L.S., Saltonstall C.B, and Feng. Y., "Thermal transport barrier in carbon nanotube array nanothermal interface materials," *Carbon,* Vol. 120, p. 120-136, 2017.

[16] Qiu, L., Guo P., Kong Q., Tan C.W., Liang K, Wei J., Tay J.N., Feng Y., Zhang X., and Tay B.K., "Coating-bousted interfacial thermal transport for carbon nanotube array nano-thermal interface materials," *URL Carbon* Vol. 145, p. 725-735,

2019.

[17] Yu W., Liu C., Qui L., Zhang P., Ma W., Yue Y., Xie H., Larkin L.S., "Advanced thermal interface materials for thermal management," *Engineering Science,* Vol. 3, No. 9, pp. 1-3, 2018.

[18] Nestereuko D.V., Lyubarskaya A.V., Kolesnikova M.D., and Soifer V.A., "The dependence of the image edge detection directivity by Brewster effect on the gradient of inhomogeneities of objects," *in Journal of physics: Conference series* Vol. 1368, 2019.

[19] Zhu T., Zhou Y., Ye H., Qiu M., Ruan Z., and Fan S., "Plasmonic computing of spatial differentiation.," *Nat. Comm.* Vol. 8, pp. 1-3, 2017.

[20] Golovastikov N.L., Bykor D.A., and Doskolovich L.L., "Temporal differentiation and integration of 3D optical pulses using phase-shifted Bragg gratings," *Computer Optics,* Vol. 1, No. 41, pp. 13-21, 2017.

[21] Nesterenko D.V, Kolesnikova M.D. and Lyubarskaya A.V., "Optical differentiation based on the Brewster effects," *Computer Optics,* Vol. 42, No. 5, pp. 758-763, 2018.

[22] Tsenova V. and Stoykova E., "Refractive index measurement in human tissue samples," *in Proc. SPIP,* pp. 413-417, 2003.

[23] Anderson R.R. and Parrish J.A., "The optics of human skin," *J. Invest. Derimatol* , Vol. 77, No. 1, pp. 13-19, 1981.

[24] Caspers P.J., Lucassen G.W., Carter E.A, Bruining H.A. and Puppels G.J., "In vivo confocal Raman microspectroscopy of the skin: Noninvasive determination of molecular concentration profiles," *J. Invest Dermatol,,* Vol. 116, No. 3, pp. 434-442, 2001.

[25] Ding H., Lu J.Q., Jacobs K.M., and Hu X.-H., "Determination of refractive indices of porcine skin tissues and Intralipid at eight wavelengths between 325 and 1557 nm," *J. Opt. Soc. Am. A,* Vol. 22, No. 6, pp. 1151-1157, 2005.

[26] Ding H., Lu J.Q., Wooden W.A., Kragel P.J., and X.-H. Hu, "Refrative indices of human skin tissue at eight wavelengths and estimated dispersion relations between 300 and 1,600 nm," *Phys. Med. Biol.,* Vol. 51, No. 6, pp. 1479-1489, 2006.

[27] Lai J.C., Zhang Y.-Y., Li Z.-H., Jiang H.-J., and He A.-Z, "Complex refractive index measurement of biological tissue by attenuated total reflection ellipsometry," *Appl. Opt,* Vol. 49, No. 16, pp. 3235-3238, 2010.

[28] Lai J., Li Z., Wang C., and He A., "Experimental measurement of the refractive index of biological tissues by total internal reflections," *Appl. Opt.,* Vol. 44, No. 10, pp. 845-1849, 2005.

[29] Song Q.W., Ku C.Y, Zhang C., Gross R.V., Birge R.R., and Michalak R., "Modified critical angle method of measuring the refractive index of bio-optical materials and its applications to bacteri-orhodospin," *J. Opt. Soc. Am. B.,* Vol. 12, No. 5, pp. 797-803, 1995.

[30] Dirkx J.J.J., Kuypers L.C., and December W.F., "Refractive index of tissue measured with confocal microscopy,," *J. Biomed Opt.,* Vol. 10, No. 4, p. 044014, 2005.

[31] Tearney G.J., Brezinski M.E., Southern J.F., Bouma B.E, Hee M.R., and Fujimoto J.G., "Determination of the refractive index of highly scattering human tissue by optical coherence tomography," *Opt. lett.,* Vol. 20, No. 21, pp. 2258-2260, 1995.

[32] Sand M., Gambichler T., Moussa G., Bechara F.G., Sand D., Altmeyer P., and Hoffmann K., "Evaluation of the epidermal refractive index measured by optical coherence tomography," *Skin Res. Technol.* , Vol. 12, No. 12, pp. 114-118, 2006.

[33] Ackermann G., Hartmann M., Scherer K., Lang E.W., Hohenleutner U., Landthaler M., and Baumler W., "Correlation betweeen light penetration into skin and the therapeutic outcome following laser therapy of port-wine stains," *Lasers. Med. Sci.* , Vol. 17, No. 2, pp. 70-78, 2002.

[34] Solan J.L. and Laden K., "Factors affecting the penetration of light through stratum corneum,," *J. Soc. Cosmet. Chem.* , Vol. 28, No. 3, pp. 114-118, 1977.

[35] Yoshida K., Ohkubo K., Ojima N., and Iwata K., "Application of the critical angle method of refractive index measurement of human skin in vivo under partial contact," *Journal of Biomedical Opts* , Vol. 18, No. 3, pp. 037002-1 to 037002-6, 2013.

[36] Furia L., Hill D.W. and Gandhi O.P., "Effects of Millimeter-Wave Irradiation on Growth of Saccharomyces cerevisiae," *IEEE Transactions on Biomedical Engineering,* Vol. 33, No. 11, 1986.

[37] Zhadobov M., Chahat N., Sauleau R., Quement C.L. and Drean Y.L., "Millimeter -wave Interactions with the Human Body: State of Knowledge and Recent Advances," *Inetrnational Journal of Microwave and Wireless Technologies* , 2011.

[38] Gandhi O.P. and Riazi A., "Absorption of Millimeter Waves by Human-beings and its Biological Implications," *IEEE Transaction on Microwave Theory and Techniques,* Vol. 34, No. 2, 1986.

[39] *IEEE Standard for Safety Levels with Respect to Human Exposure to the Radio Frequency*

Electomagnetic Fields, 3 kHz to 300 GHz. IEEE Standard C951, 2005

[40] Tissue Properties, ITIS Swiss, [Online]. Available: www.itis.swiss [Accessed 17 May 2024].

[41] Body Tissue Dielectric Parameters, Federal Communications Commission, [Online]. Available: www.fcc.gov/general/body [Accessed January 18, 2024].

[42] Wu T., Rappaport T.S., and Collins C.M., Safe for generations to come: Considerations of Safety for Millimeter Waves in Wireless Communications. *IEEE Microwave Magazine*, Vol. 16, No. 2, pp. 65-84, 2015.

[43] Collins C.M., Liu W., Wang J., Gruetter R., Vaughan J.T., Ugurbil K. and Smith M.B., "Temperature and SAR calculations for a human head within volume and surface coils at 64 and 300 MHz", *J. Magn. Reason Imaging*, Vol. 19, No.5, pp. 650-659, 2004.

[44] Cancer Society, New Zealand. www.cancer.org.nz [Accessed October, 24, 2023].

Godday Biowei received B.Eng. degree in Electrical and Electronic Engineering from Niger Delta University, Bayelsa in 2007, MSc. in Electronic Communications and Computer Engineering in 2010 from Nottingham University UK and Ph.D. degree from Niger Delta University, Bayelsa in 2024.
He is currently affiliated with the Niger Delta University, Wilberforce Island, Bayelsa. His areas of interest include electromagnetics, communication systems and wave propagation.

Sulaiman Adeniyi Adekola took his B.Sc. degree in Electrical Engineering from the Ahmadu Bello University in Zaria, Nigeria (1968), and the degree of M.Sc. (1972) and Ph.D. (1975) both in Electrical Engineering from the Ohio State University, Columbus, Ohio, USA. He was between 1976 and 2010 teaching at the University of Lagos, where he carried out research in his major fields of acoustic (echosonde) antennas, electromagnetics, and propagation of radio waves. He is an Emeritus Professor in Electrical and Electronics Engineering of the University of Lagos and is Fellow of a number of professional bodies including the IET (FIET).

Kamoli Akinwale Amusa received the B.Eng., M.Sc. and Ph.D. degrees in Electrical and Electronic Engineering, from the University of Ilorin, Ilorin, University of Lagos, Lagos and Federal University of Agriculture, Abeokuta, all in Nigeria, in 1999, 2011, and 2017 respectively.
His major field of study is communications engineering and digital signal processing. He has published few papers on antennas, communications, and signal processing. His current research interests include electromagnetic fields, microwave engineering, antennas, wave propagation and signal processing.